

The decay dynamics of photoexcited rare gas cluster ions

A. B. Jones, P. R. Jukes, and A. J. Stace

Citation: *The Journal of Chemical Physics* **111**, 959 (1999); doi: 10.1063/1.479378

View online: <http://dx.doi.org/10.1063/1.479378>

View Table of Contents: <http://scitation.aip.org/content/aip/journal/jcp/111/3?ver=pdfcov>

Published by the [AIP Publishing](#)

Articles you may be interested in

[Coulomb explosion in dicationic noble gas clusters: A genetic algorithm-based approach to critical size estimation for the suppression of Coulomb explosion and prediction of dissociation channels](#)

J. Chem. Phys. **132**, 234104 (2010); 10.1063/1.3439690

[Theoretical modeling of postionization fragmentation of rare-gas trimer cations](#)

J. Chem. Phys. **125**, 104315 (2006); 10.1063/1.2337632

[Structural transitions in metal ion-doped noble gas clusters: Experiments and molecular dynamics simulations](#)

J. Chem. Phys. **108**, 4450 (1998); 10.1063/1.475856

[Collisions of rare gas ions with C 60 : Endohedral formation, energy transfer, and scattering dynamics](#)

J. Chem. Phys. **107**, 8370 (1997); 10.1063/1.475037

[Covariance images of the primary response from rare gas cluster ions to photoexcitation](#)

J. Chem. Phys. **106**, 1367 (1997); 10.1063/1.473305



The decay dynamics of photoexcited rare gas cluster ions

A. B. Jones, P. R. Jukes, and A. J. Stace^{a)}

School of Chemistry, Physics and Environmental Science, University of Sussex, Falmer, Brighton BN1 9QJ, United Kingdom

(Received 25 February 1998; accepted 20 April 1999)

The kinetic energies of fast neutrals ejected from photoexcited rare gas cluster ions have been measured for the following systems: Ar_n^+ , Kr_n^+ , Xe_n^+ at two photon wavelengths: 355 and 532 nm, and for n in the range 2–19. New data are presented for xenon at both wavelengths, and for argon and krypton cluster ions at 355 nm. For argon and krypton cluster ions at 532 nm, new data have been recorded which are more accurate than those presented previously. A Monte Carlo model of the experiment has been used to simulate the kinetic energy releases and also to investigate variations in the scattering anisotropy parameter (β) as a function of photon energy and cluster composition and size. Significant fluctuations in β are observed, and these are attributed to a combination of structural variation and changes to the nature of the central chromophore. For small cluster ions the kinetic energy release data show evidence of being influenced by the final spin-orbit state of the atomic ion. Overall, there is a gradual decline in kinetic energy release as a function of increasing cluster size; however, there are marked variations within this trend. For all three rare gas systems the results show that the primary response to photoexcitation is the ejection of a single atom with a high kinetic energy on a time scale that is short compared with the rotational period of a cluster. © 1999 American Institute of Physics. [S0021-9606(99)00627-3]

I. INTRODUCTION

The photoexcitation of rare gas cluster ions of the form Ar_n^+ , Kr_n^+ etc. at ultraviolet (UV) and visible wavelengths can be a very destructive process in which a small ionic photofragment is accompanied by large numbers of neutrals, most probably in the form of atoms.¹ Early studies of the energetics of such processes concentrated on ionic photofragments and, most notably, a number of groups measured the distribution of laboratory frame kinetic energy for Ar^+ from Ar_3^+ , with the observation that it consists of two components.^{2–5} First, there are ions that emerge from the dissociation process with comparatively high energies; these are scattered anisotropically and, as such, exhibit a marked dependence on the angle of polarization of the laser radiation with respect to the flight direction of the ion beam. A second component consists of ions with relatively low kinetic energies and these appear to be scattered isotropically. However, as the cluster ions increase in size it is found that ionic photofragments cease to show evidence of a high kinetic energy component,^{6,7} and beyond $n=6$ features due to anisotropic scattering are no longer detectable.⁶

Subsequently, new experiments were developed to measure the neutral products of photo-induced decay in order to determine how energy is being dissipated in larger cluster ions.^{7–11} These experiments use time-of-flight (TOF) techniques to measure the arrival times of the neutrals, and it is observed that, following photodissociation, fast neutral atoms appear in the form of anisotropic wings at positions which correspond to either forward or backward scattered events with respect to an intense central isotropic peak.^{7–11} These fast neutral atoms are ejected from clusters on a time

scale which is less than one rotational period (10–50 ps),¹² and carry with them up to 50% of the excess internal energy. Such events have been detected from clusters containing up to 25 argon atoms.⁷ Results for krypton clusters demonstrated that the earlier pattern of behavior was repeated for ions up to Kr_{25}^+ .¹⁰ In all cases the remaining internal energy is dissipated by the loss of further neutral fragments with low relative kinetic energies. Overall, these new experiments show that neutral detection provides a subtle probe of the decay dynamics of fragile rare gas cluster ions.

In this paper new data are presented for the Xe_n^+ series of cluster ions. In addition, improved measurements have been undertaken on the photofragmentation of Ar_n^+ and Kr_n^+ clusters at 532 nm, and a limited number of new results are presented following the excitation of small cluster ions from all three rare gases at 355 nm. This series of measurements provides the bases for a quantitative analysis of energy partitioning and scattering in terms of a dynamical model designed to simulate the experimental environment. Of particular interest from these calculations are the dependencies of kinetic energy release and anisotropy parameter, β , on cluster size. These quantities have been determined from simulations of the anisotropic scattering patterns of fast neutrals from Ar_n^+ ($n=2–21$), Kr_n^+ ($n=2–14$), and Xe_n^+ ($n=2–11$).

II. EXPERIMENT

A Vacuum Generators ZAB-2F double focusing mass spectrometer has been adapted to accommodate a supersonic cluster source and used in conjunction with a TOF apparatus to perform the experiment reported here. Details of a similar apparatus have been presented earlier,^{7,10,13} and Fig. 1 gives a schematic diagram of the experimental configuration.

^{a)}Electronic mail: A.J.Stace@sussex.ac.uk

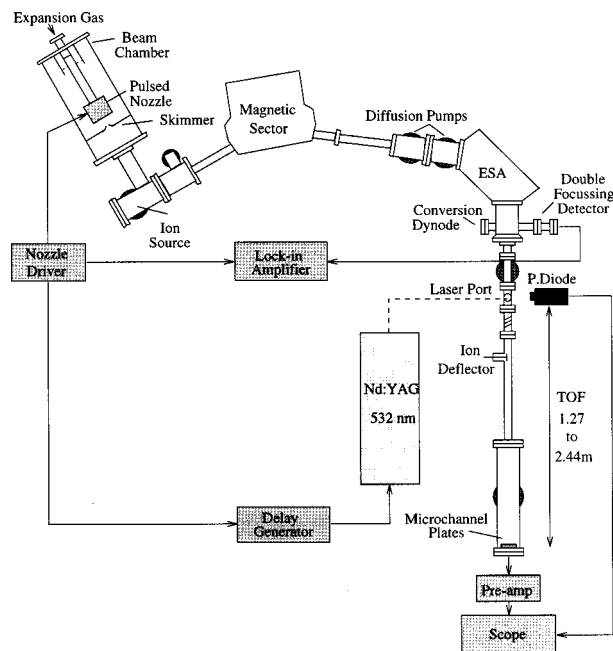


FIG. 1. A schematic diagram of the apparatus.

Briefly, a beam of clusters is produced from an adiabatic expansion of the pure gas through a pulsed conical nozzle 200 μm in diameter. The beam is collimated by a 1 mm diameter skimmer and passes into the ion source of the ZAB-2F, 55 cm downstream from the nozzle. A parent ion is accelerated to a laboratory-frame kinetic energy of between 4 and 8 keV and is mass- and kinetic energy-resolved before entering the TOF device. The detected ion signal on the microchannel plate detector (MCP) at the end of the TOF tube is maximized by adjusting various focusing and steering voltages sited throughout the mass spectrometer. Thus the ions (and hence, the neutrals) are on trajectories which bring them to a focus at the final detector. The alternative would be to bring the ion beam to a focus where it interacts with the laser; however, beyond that point the ion beam would begin to diverge and there would be a subsequent loss of time resolution at the detector. Size-selected cluster ions are photodissociated by a 10 ns pulse from an unfocused frequency-doubled (532 nm) or tripled (355 nm) Nd:yttrium-aluminum-garnet at the entrance of the 1.44 m length flight tube. The laser beam is collimated to give a rectangular beam of dimensions (1 \times 6 mm), with the shorter dimension lying parallel to the ion flight axis. Collimation increases the resolution of the experiment, since the width of the photofragment pulse contributes to the spread of arrival times at the MCP. A further 20 cm beyond the point of laser interaction, all remaining ions are deflected by a plate raised to a voltage of 5 kV, allowing only neutral species to continue along the flight tube. A pressure of 10^{-8} mbar is maintained in the flight tube to keep the probability of collisions to a minimum. After passing through a pre-amplifier (EG&G Ortec VT120), the output from the MCP is collected as an arrival time distribution on a multichannel scalar (MCS) (Stanford model SR 430). The MCS acquires data not by

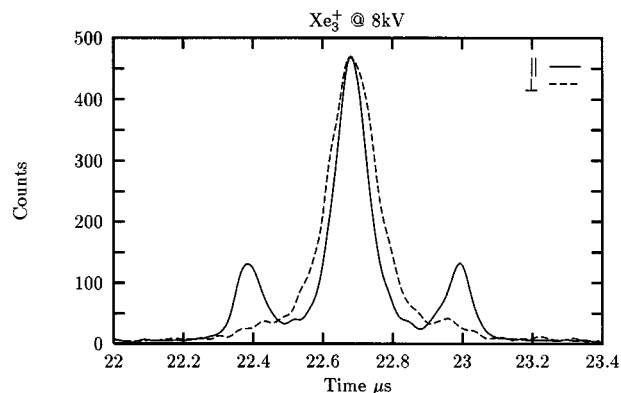


FIG. 2. Distribution of arrival times for neutrals following the photofragmentation of Xe_3^+ at 532 nm. Data were recorded for two orientation of laser polarization with respect to the ion beam: parallel polarization shown thus: —; perpendicular polarization shown thus: - - -.

averaging but by accumulation into 5 ns time bins, and the signal to noise ratio is controlled by the adjustment of an internal discriminator.

To increase the detected neutral fragment yield from ions with low intensities, 40 ns bins were used, which resulted in a reduction in time resolution. However, because the decline in intensity was frequently accompanied by an increase in mass, the drop in resolution when using 40 ns bins was not too dramatic. One advantage of the TOF device is its lack of sensitivity to isotopes,⁹ which allows the accumulation of signal from parent ions, such as Kr_n^+ and Xe_n^+ , to proceed with minimal loss of time resolution. Data from krypton and xenon clusters have been analyzed using the isotopic average masses of 83.4 and 131.06 amu, respectively.

A typical experimental result is shown in Fig. 2 for Xe_3^+ photodissociated at 532 nm. The two arrival time profiles for neutral atoms were recorded with the plane of polarization of the laser radiation either parallel or perpendicular to the ion flight direction. When the plane of polarization is parallel to the ion flight direction (solid line), two wings are observed at ~ 22.4 and $\sim 23 \mu\text{s}$, which undergo a marked reduction in intensity when the plane of polarization is rotated by 90° (dashed line). Such behavior is indicative of a rapid decay process that proceeds on a time scale ($\sim 10^{-12}$ s) which is short in comparison to the rotational period of the cluster (see later). However, it is evident from Fig. 2 that the wings do not disappear completely when the laser radiation is orientated at 90° with respect to the ion beam, and the source of this residual signal will be discussed later. In addition to the fast process identified earlier, the arrival time profile is dominated by an intense central feature which corresponds to the slow loss of atoms from the excited cluster. Numerous examples of these profiles have been given previously and they all follow the basic structure shown in Fig. 2,^{7,8} i.e., low intensity wings corresponding to a single fast atom either forward- or backward-scattered, accompanied by an intense central feature which can be attributed to the gradual loss of large numbers of atoms with low kinetic energies.

Neutral photofragments acquire relative kinetic energy

from the dissociation process which leads to a spread in velocities, and hence, arrival times at the detector. For the process



the average kinetic energy release T_n can be calculated from the time difference between the two wings (Δt) using the following expression⁶

$$T_n = \frac{M_3}{2M_1M_2} \left[\frac{\Delta t E_0}{L} \right]^2, \quad (2)$$

where M_1 , M_2 , M_3 are the masses of the initial ion, the ionic photofragment(s) and the neutral photofragment(s), respectively, E_0 is the ion source acceleration voltage, and L is the length of the flight tube. The kinetic energy resolution of the TOF device is given by the expression⁶

$$\delta T_n = \frac{E_0 \delta t T_n^{1/2}}{L} \left[\frac{2M_3}{M_1M_2} \right]^{1/2}, \quad (3)$$

where δt is the time resolution of the experiment, which from "hole burning" studies of ion profiles, is estimated to be ~ 30 ns for this series of experiments.¹⁰ The nature of Eq. (3) is such that small kinetic energy releases can be measured very accurately, but the resolving power of the TOF device drops markedly as the magnitude of T_n increases.

III. A COMPUTER MODEL OF THE EXPERIMENT

Although the arrival time profiles provide a qualitative picture of the angular distribution of products following prompt photodissociation, they represent a convolution of molecular and instrumental factors, and the latter can have a significant effect on determining peak shape. To take account of experimental parameters, a Monte Carlo model of the TOF section of the experiment has been developed to simulate individual photodissociation events. Monte Carlo sampling methods were used to superimpose a center of mass distribution of ion photodissociation products onto a laboratory-frame coordinate system in order to determine whether or not individual neutral photofragments would hit the detector. For a cluster ion with transition dipole μ orientated parallel to the polarization vector of the laser radiation, ϵ , the angular distribution of photofragments is given by the standard equation^{14,15}

$$P(\theta) = \frac{1}{4\pi} [1 + \beta P_2(\cos \theta)], \quad (4)$$

where θ is the angle between ϵ and the fragment velocity vector, v , and P_2 is a second degree Legendre polynomial. β is the anisotropy parameter and is a measure of the correlation between μ and v . This correlation can be expressed in the form of an expectation value

$$\beta = 2 \langle P_2(\cos \chi) \rangle, \quad (5)$$

where χ is the angle between μ and v . Thus β has limiting values $-1 \leq \beta \leq 2$ with $\beta = -1$ for $\mu \perp v$ ($\chi = 90^\circ$) and $\beta = 2$ for $\mu \parallel v$ ($\chi = 0^\circ$). These limiting values are only applicable under circumstances where the dissociation time scale is much shorter than the rotational period of the parent cluster ion.

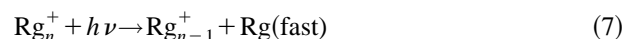
The corresponding scattering distribution then takes one of two forms: $\beta = 2$ gives a $\cos^2 \theta$ distribution and $\beta = -1$ gives a $\sin^2 \theta$ distribution. As a measure of the time scale of events, β can also be expressed¹⁶ in terms of the following relationship between the decay time of the photoexcited state (τ) and the angular frequency (ω) for a cluster of a given size

$$\beta = 2P_2(\cos \chi) \left[\frac{1 + \omega^2 \tau^2}{1 + 4\omega^2 \tau^2} \right]. \quad (6)$$

A qualitative description of Fig. 2 in terms of the preceding discussion would propose that the intense central feature is due to the isotropic scattering of atoms ($\beta \approx 0$) and that the wings are due to an anisotropic scattering process (β in the range 1–2).

Using Monte Carlo methods, numerical simulations have been performed with the objective of reproducing the results obtained from each experiment. The primary purpose of this exercise was to extract from the experimental data kinetic energy distributions associated with the anisotropic features seen in the arrival time profiles of the neutral photofragments. The model used as input: (1) the masses of the parent ion and two fragments; (2) a typical value for the variation (uncertainty) in the ion beam kinetic energy (~ 10 eV); (3) the acceleration voltage of the ion source; (4) the radius of the MCP; (5) the length of the flight tube; (6) the width of the laser/ion beam cross section; (7) the angle of polarization of the laser beam with respect to the ion beam (0° or 90°); and (8) the anisotropy parameter β . Finally, an initial guess as to the shape of the kinetic energy release distribution is required, and for the purposes of importance sampling, a three-variable triangular distribution was used. Since the mode of fragmentation responsible for the wings shown in Fig. 2 is unlikely to be statistical, there is no *a priori* method for determining the shape of the kinetic energy distribution, and a triangle proved to yield the best fit to most of the experimental data.

In a recent experiment,¹⁷ coincidence techniques were used to demonstrate that the primary response from rare gas cluster ions $n \geq 4$, to photoexcitation, is the ejection of a single atom with a high kinetic energy as opposed, for example, to the loss of two fast atoms in opposite directions. It was possible to establish that this mode of decay was present in both argon and krypton cluster ions containing up to 10 atoms.¹⁷ In the calculations which follow the coincidence result has been used as the bases of our analysis of all the neutral atom arrival time profiles recorded for all cluster ions discussed here. Therefore, the model assumes that the reaction step responsible for each set of high energy wings is¹⁷



and performs Monte Carlo averages over the parameters listed earlier in order to reproduce the appropriate sections of experimental data. It is acknowledged that the smaller cluster ions, Rg_3^+ and Rg_4^+ exhibit fragmentation patterns which are more complex than that represented by Eq. (7). Examples of these can be seen in the work of Nagata *et al.*⁵ and the competing fragmentation pathways seen for Ar_3^+ , in particular, have been the subject of much debate.^{2–5} Equation (7) is

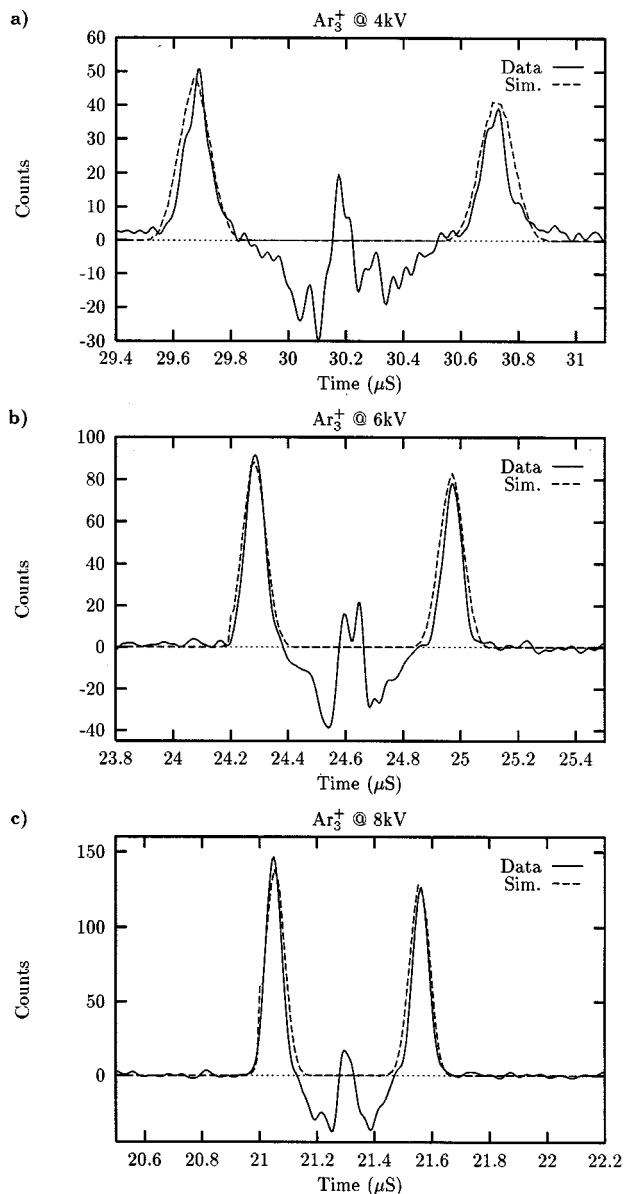


FIG. 3. Arrival time distributions for fast neutral atoms resulting from the photofragmentation of Ar_3^+ at 532 nm. The profiles shown as solid lines result from the subtraction of data sets recorded for parallel and perpendicular orientations of laser polarization. The dashed lines are simulated fits to the data where the only variable is the laboratory-frame kinetic energy of the ion (see text for further details).

taken to represent a decay route that is common to the majority of cluster ions studied in this series of experiments.

IV. RESULTS

Two separate time-resolved distributions of photoneutrals were recorded for each cluster ion studied, and these corresponded to angles of laser polarization of 0° and 90° with respect to the ion beam. Typical examples of arrival time profiles are given in Fig. 2, and these results will be used to illustrate how all of the data sets have been processed. Of primary interest are the two wings seen at ~ 22.4 and $\sim 23 \mu\text{s}$ as these correspond to the ejection of single atoms with high kinetic energies. In order to improve the accuracy of measurements made on the time separation of

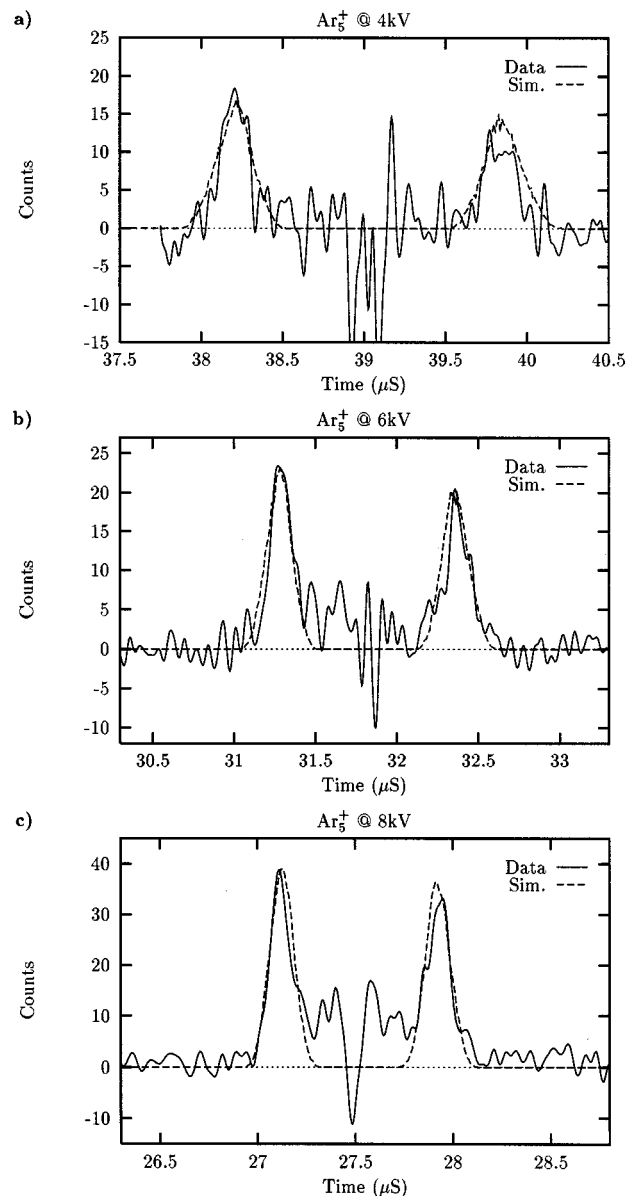


FIG. 4. As for Fig. 3, but experimental and simulated results for Ar_5^+ .

the wings [Δt in Eq. (2)], profiles of the type shown in Fig. 2 were normalized with respect to the central isotropic feature and then subtracted from one another. This procedure is effective because the central feature in each profile is due to the isotropic scattering of atoms with low kinetic energies. Figure 3 shows the results obtained when a similar procedure is applied to data recorded for Ar_3^+ . The residual features are due to small fluctuations in signal intensity and/or the trigger timing signal received by the MCS.

The subtraction leaves behind the anisotropic high energy wings, which can then be studied in isolation from the more intense isotropic component. All subsequent examples of arrival time profiles correspond to subtracted data sets that have been treated in a manner similar to that described earlier for Xe_3^+ . Data sets obtained in this way were fitted using the simulation procedure discussed in Sec. III, and a mean kinetic energy release determined for reaction (1) from all cluster ions. With the exception of dimer ions, the simula-

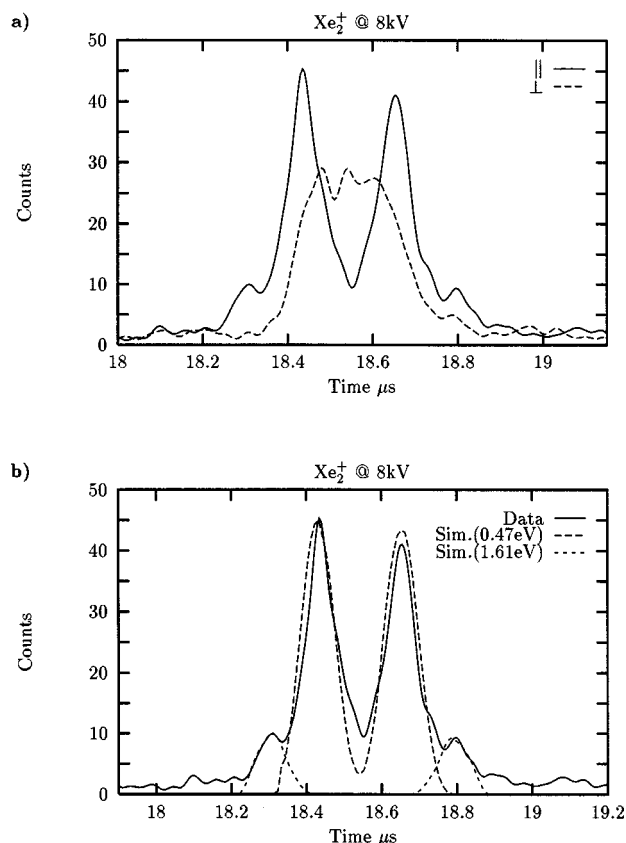


FIG. 5. (a) As for Fig. 2, but for Xe_2^+ at two different angles of laser polarization; and (b) as for Fig. 2, but for Xe_2^+ with the laser orientated parallel to the ion flight direction, and includes the results of a computer simulation. In both cases, the presence of two sets of wings is clearly visible, and these are due to different spin-orbit states of the Xe^+ photofragment being populated.

tions were fitted to the subtracted data sets by inspection. The variations in average kinetic energy when using such a method were found to be less than 10%. For dimer ions, the simulations were fitted directly to distributions obtained by recording data with the angle of polarization of the laser radiation orientated parallel to the ion beam.

For the computer model to be valid, it should be capable of reproducing data recorded under a variety of experimental conditions. For specific cluster ions, experimental data sets were recorded under identical conditions, except for a systematic variation in the laboratory-frame kinetic energy of the parent cluster ion (E_0). Figures 3 and 4 show subtracted data sets for Ar_3^+ and Ar_5^+ , respectively, where in each case a simulation has been performed with E_0 fixed at 6 keV. To fit the remaining distributions, the only variable adjusted was E_0 to either 4 or 8 keV, as required by the experiment. It can be seen from the results, that the model is able to provide a quantitative fit to the arrival time distributions at each different laboratory-frame kinetic energy. A further measure of the consistency exhibited by the model, is obtained when the center of mass kinetic energy distributions of neutrals are compared for the different experimental conditions. When all three simulation results were normalized the kinetic energy release distributions were found to be identical.¹⁸

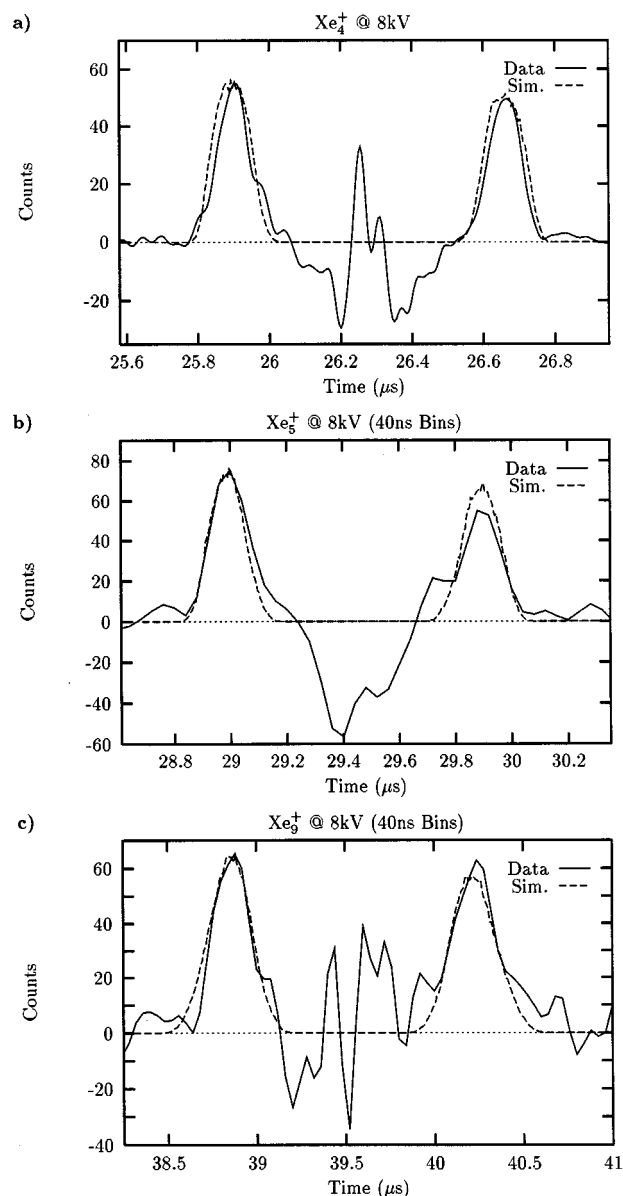


FIG. 6. As for Fig. 3, but for (a) Xe_4^+ , (b) Xe_5^+ , and (c) Xe_9^+ .

A. Xenon cluster ions at 532 nm

An interesting feature of this series of experiments is the behavior of Xe_2^+ . Under circumstances where ϵ is parallel to the ion flight direction Fig. 5 shows two pairs of clearly distinguishable wings, which correspond to neutrals with quite different kinetic energies. Such behavior can be attributed to the effects of spin-orbit coupling on both the Xe_2^+ electronic energy levels, and the final electronic state of the Xe^+ product, which can be either $^2P_{3/2}$ or $^2P_{1/2}$. The model yields a mean kinetic energy release of 1.61 eV for the most energetic neutrals and a value of 0.47 eV for the low energy component. Given that the bond energy for the xenon dimer ion is 1.03 eV, the recorded kinetic energy release is larger than would be expected for a 2.33 eV photon. The discrepancy is probably due to photoexcitation out of a vibrationally excited state of the electronic ground state. The simulated results are shown in Fig. 5(b), and yield a difference between the two energy releases of 1.14 eV, which is to be compared

TABLE I. Summary of the average values for kinetic energy release derived from Monte Carlo simulations of the experimental data.

Cluster (<i>n</i>)	Center of mass kinetic energy release (T_n)/eV					
	Photon energy 2.33 eV			Photon energy 3.5 eV		
	Ar _{<i>n</i>} ⁺	Kr _{<i>n</i>} ⁺	Xe _{<i>n</i>} ⁺	Ar _{<i>n</i>} ⁺	Kr _{<i>n</i>} ⁺	Xe _{<i>n</i>} ⁺
2	1.24	0.88	1.61
3	0.62	0.67	0.83	1.34	1.14	0.77
4	0.50	0.58	0.64	0.51	0.63	...
5	0.45	0.51	0.54	0.43
6	0.45	0.46	0.48
7	0.44	0.41	0.42
8	0.44	0.39	0.40
9	0.50	0.38	0.34
10	0.46	0.35	0.35
11	0.46	0.35	0.35
12	0.46	0.43
13	0.43	0.37
14	0.43	0.42
15	0.41
16	0.36
17	0.38
18	0.41
19	0.42

^aDue to population of the Xe⁺(²P_{1/2}) spin-orbit state.

with a spin-orbit splitting in Xe⁺ of 1.31 eV. Again, this mismatch is probably due to each excitation step sampling from a different region of the ground state vibrational manifold for Xe₂⁺.

Typical TOF distributions for Xe₃⁺ were presented earlier in Fig. 2 where high energy wings due to the anisotropic scattering of photofragments are clearly visible. The resolution of the mass spectrometer was degraded in order to transmit neighboring isotopic combinations so as to increase parent ion intensity. The measurements were not helped by the fact that the absorption cross section for Xe₃⁺ is an order of magnitude lower at 532 nm (2.33 eV) than at its peak at 690 nm (1.8 eV).¹⁹ Further examples of subtracted experimental arrival time profiles for larger xenon cluster ions are plotted together with the results of computer simulations in Fig. 6. Note the use of 40 ns time bins to record events from the larger clusters ions.

The mean kinetic energy releases deduced from the experiments using computer simulations are given in Table I. For Xe₃⁺ the mean kinetic energy at 532 nm is 0.83 eV, which appears high, when compared with values determined for Ar₃⁺ and Kr₃⁺ at 0.62 and 0.67 eV, respectively. Recent work by Haberland, Hofmann, and von Issendorff¹¹ on rare gas trimer ions suggests that at a photon energy of 2.33 eV (532 nm), the only transition to be excited in Xe₃⁺ is $\Pi(1/2)_g \leftarrow \Sigma(1/2)_u$, which in turn means that the atomic ion appears in the ²P_{3/2} state. Haberland, Hofmann, and von Issendorff¹¹ infer that the slow and fast neutrals detected are therefore accompanied only by fast ions. Crossing to the $\Pi(1/2)_u$ excited state of Xe₃⁺ (the route to slow ions) is unlikely at this photon energy, and calculations show the charge in the $\Pi(1/2)_g$ state to reside on the outer atoms. A similar conclusion regarding the final state of the atomic ion

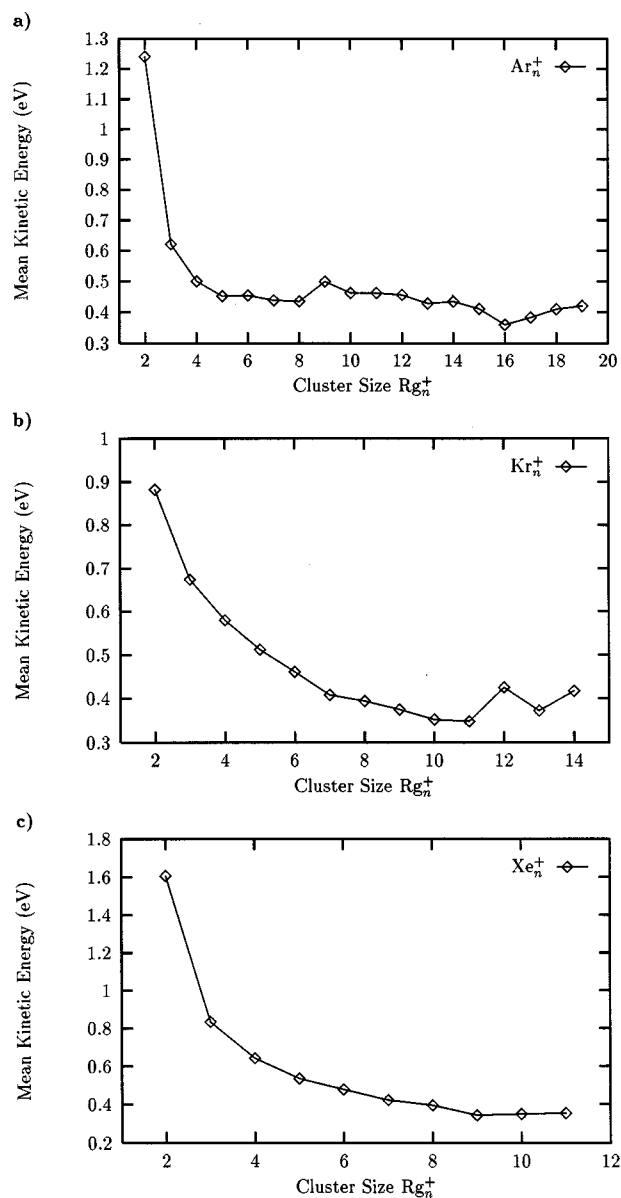


FIG. 7. Mean center of mass kinetic energy releases for fast neutral atoms, as derived from computer simulations of the type shown in Figs. 3–6. Additional examples for krypton cluster ions are presented later in the text.

can be reached from considerations of energy balance. Since the binding energy of Xe₃⁺ is ~1.24 eV, the magnitude of the kinetic energy release at 532 nm (2.33 eV) is sufficiently large as to make it impossible for the final spin-orbit state of Xe⁺ to be anything other than ²P_{3/2}.

Fast neutrals were seen to be ejected from xenon clusters up to *n* = 11, and although it is thought that this trend continues in larger ions, such events could not be detected because of very low signal intensities. From the mean kinetic energies of the fast neutrals shown in Table I it can be seen that the xenon cluster series exhibits a steady reduction in energy release with increasing size, with the exception of *n* = 10 where there is a small rise. The overall pattern of behavior is concurrent with an increased capacity for energy dissipation as the number of degrees of freedom increases. For comparison with the other rare gas systems discussed

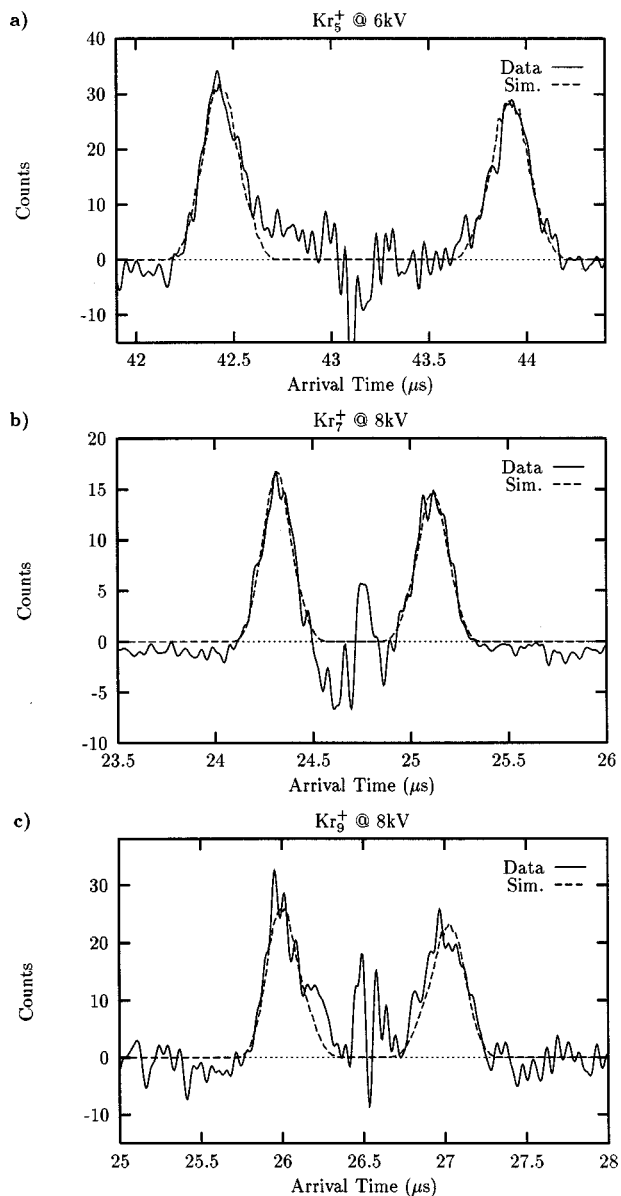


FIG. 8. As for Fig. 3, but for (a) Kr_5^+ , (b) Kr_7^+ , and (c) Kr_9^+ .

later, the data for xenon are plotted in Fig. 7 as a function of cluster size.

B. Argon and krypton cluster ions at 532 nm

New data were recorded for Ar_n^+ cluster ions, where $n = 2$ to 19,⁷ and examples of subtracted arrival time profiles together with simulated fits were shown earlier in Figs. 3 and 5. The kinetic energy releases deduced from the model are summarized in Table I and are also presented graphically in Fig. 7, where it can be seen that the general trend in kinetic energy release as a function of size is downwards, with slight fluctuations observed for $n = 9$ and 16.

The computer model has also been used to analyze new data recorded at 532 nm for krypton cluster ions, Kr_n^+ , for n in the range 2–14.¹⁰ Examples of experimental data together with simulated fits are given in Fig. 8, and the mean kinetic energies are given in Table I and shown graphically in Fig. 7. As for xenon and argon, the general trend is for the kinetic

energy release to decrease as the ions increase in size. However, given that the mass of the precursors and fragments are all very different, there is a remarkable similarity in the magnitudes of the kinetic energy releases from all three rare gases for $n \geq 4$.

The comparatively low value recorded for the kinetic release of photofragments from Kr_2^+ would suggest the participation of the excited spin-orbit state in the dissociation step. The value given in Table I is comparable to that recorded by Abouaf *et al.*²⁰ at 531 nm for the $2(1/2)_g \leftarrow 1(1/2)_u$ transition in which Kr^+ is formed in the excited spin-orbit state. A further observation to emerge from the work of Abouaf *et al.*²⁰ is the presence of a single transition at 531 nm, which would explain the absence of any structure in the arrival time profile associated with the formation of Kr^+ in the lower $^2P_{3/2}$ state. This pattern of behavior contrasts with that discussed earlier for Xe_2^+ . For Kr_3^+ the situation is reversed; the total binding energy of the ion is ~ 1.37 eV and the only process observed following photoexcitation is $\text{Kr}_3^+ \rightarrow \text{Kr}^+ + 2\text{Kr}$.²¹ Hence, an energy release of 0.67 eV would leave the atomic ion with insufficient energy to populate the upper spin-orbit state. This conclusion was discussed in detail previously,¹⁰ and the new data presented here confirms that analysis. Unfortunately, the spin-orbit splitting in Ar^+ is too small to allow for an accurate identification of the final state of the ion following the photodissociation of Ar_3^+ . However, the results of Harberland, Hofmann, and von Issendorff¹¹ would suggest that it is the lower $^2P_{3/2}$ state that is populated in the Ar^+ photofragment at a photon energy of 2.33 eV.

The kinetic energy release distributions derived from the model for the Rg_3^+ and Rg_6^+ clusters are shown in Fig. 9, and separate profiles showing examples chosen from each rare gas series are given in Fig. 10. Most noticeable is the marked difference between the kinetic energy release distribution recorded for Xe_3^+ and the other two rare gas ions. What it is difficult to derive from these particular experiments, is a precise picture of the complete energy partitioning process. It is known that for all three trimer ions, photofragmentation is also accompanied by the appearance of fast and/or slow ions,^{2–7} the ratios of which can vary as a function of laser wavelength.⁶ Therefore, a complete picture of energy partitioning in the trimer ions requires that the kinetic energies of at least two of the three particles be measured in coincidence.²² In the case of a clear energy deficit, assumptions can be made regarding the final state of the ion; however, as the energy of the photon is increased (see later) the picture becomes more ambiguous.

C. Photodissociation at 355 nm

Using a photon energy of 3.5 eV (355 nm in the UV), it was possible to change the nature of the excitation step. The most obvious example is Xe_3^+ . At a photon energy of 3.5 eV, the high-energy component of the neutral atom distribution was calculated to correspond to a mean energy release of 0.77 eV. From Table I it can be seen that, in comparison to the result recorded at 532 nm, excitation at 355 nm results in less energy being released to the fast atoms. The most prob-

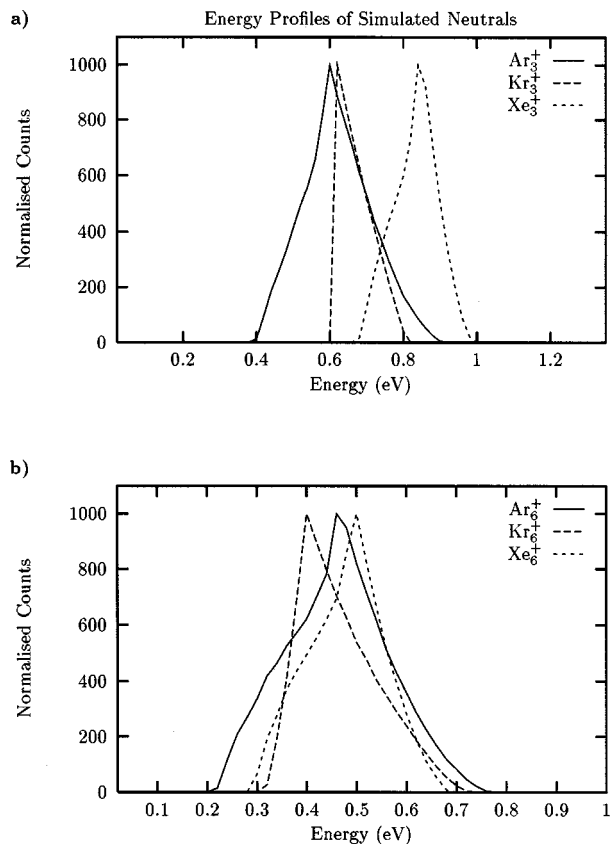


FIG. 9. Distributions of center of mass kinetic energy releases for fast neutrals as derived from the computer simulation of experimental data for (a) Ar_3^+ , Kr_3^+ , and Xe_3^+ and (b) Ar_6^+ , Kr_6^+ , and Xe_6^+ .

able explanation for this behavior is that the transition promoted is one which places the product Xe^+ in the higher spin-orbit state, leaving less energy available for the fast neutrals. This observation would match with the proposal by Harberland, Hofmann, and von Issendorff¹¹ that at 355 nm there is sufficient energy to excite Xe_3^+ to the $\Pi(1/2)_g$ excited state, where it can either stay or undergo a surface crossing to the $\Pi(1/2)_u$ state. In either case the ion dissociates to yield $\text{Xe}^+(^2P_{1/2})$.

Compared with the trimer ions, when $n=4$ and 5, the kinetic energies of the fast neutrals from both krypton and argon are seen in Table I to drop dramatically, and become comparable to those values recorded for the same ions at 2.33 eV (532 nm). Clearly there are more degrees of freedom over which Kr_4^+ can dissipate energy when compared with Kr_3^+ , however, in the absence of spin-orbit excitation, the unseen ion would have to carry away ~ 1.3 eV. Conservation of momentum would also require some of that energy to appear in the slow neutrals, which is obviously not happening. From data presented by Chen *et al.*,²¹ we would conclude that at 355 nm Kr^+ is the principle ion product, and that based on energy balance, there is sufficient energy available for the ion to emerge in the $^2P_{1/2}$ state. From an analysis of kinetic energy release measurements following the formation of Kr_2^+ as a photoproduct at longer wavelengths, Chen *et al.*²¹ concluded that Kr_4^+ is linear. If at 355 nm, $\text{Kr}^+(^2P_{1/2})$ is the first photofragment to emerge from Kr_4^+ , then the observation of the excited spin-orbit state would

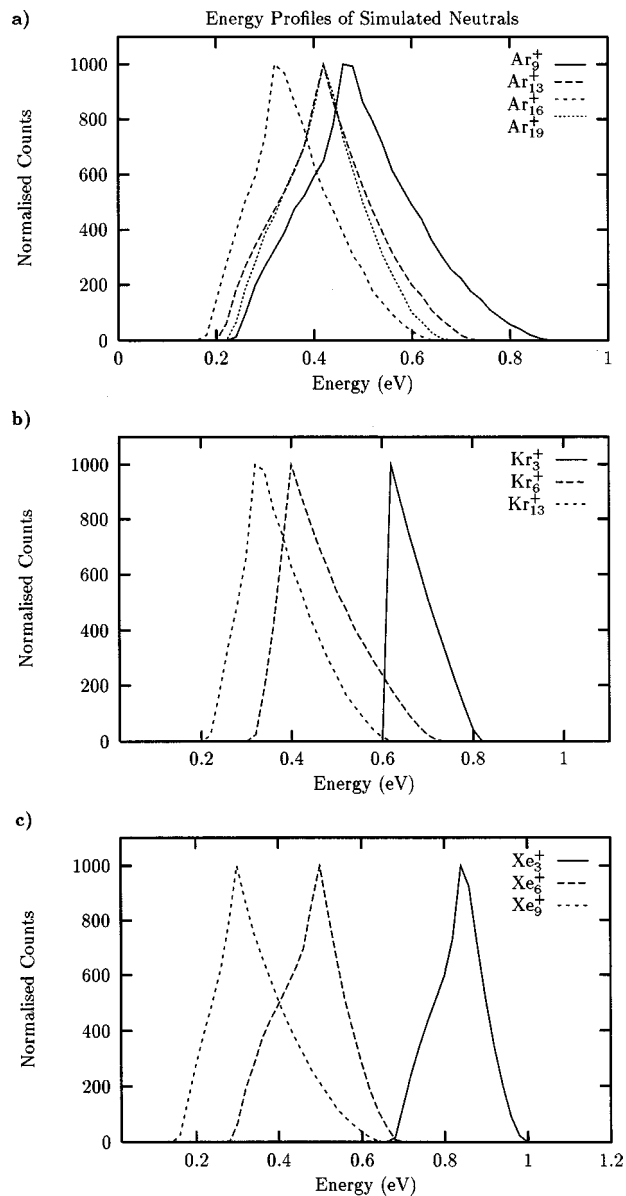


FIG. 10. Distributions of kinetic energies for fast neutrals as derived from the computer simulation of experimental data for: (a) Ar_3^+ , Ar_9^+ , and Ar_{19}^+ ; (b) Kr_3^+ , Kr_6^+ , and Kr_{13}^+ ; and (c) Xe_3^+ , Xe_6^+ , and Xe_9^+ .

support the conclusion of a linear tetramer. If instead, $\text{Kr}^+(^2P_{1/2})$ emerges after a series of fragmentation steps, then all we can conclude is that one of the ions in that sequence is linear.

V. DETERMINATION OF β

As the model incorporates a dependence on β , the anisotropy parameter, it has been possible to investigate the effect different values have on the distribution of fast neutrals. However, problems with normalization arise because of the consequences of core sampling. The size of the MCP detector is very small compared with the dimensions of the envelope of scattered neutrals when it reaches the end of the TOF tube. Hence, atoms which have high kinetic energies contribute to wings when either the scattering distribution is isotropic,²³ or when the orientation of the angle of laser po-

larization is perpendicular to the ion flight direction. Although in the latter circumstances, high energy neutrals are being ejected in a direction that is predominantly orthogonal to the direction of the detector, a small fraction of the total scattering intensity falls onto the face of the detector. However, the resultant features are weak compared to those seen when the laser radiation is polarization parallel to the direction of the ion beam. The computer model correctly predicts the presence of all the features discussed earlier.

These observations make it difficult to determine β simply by reproducing data of the type shown in Figs. 3 or 4, because it is not possible to normalize the calculated signal intensities in the wings. As a result, it was necessary to evaluate β using a method which combines both theory and experiment in a determination of the ratio of events that contributed to the wings at each orientation of the laser radiation (either parallel or perpendicular). The area under each wing in the experimental distributions was obtained by integrating over the range of arrival times covered for each laser orientation. The ratios of the two experimental areas were found to vary between 1 and 10. The comparable distributions were then simulated for each size of cluster ion at both polarizations and for a range of beta values lying between -1 and 2 in increments of 0.1. Two sample sets of calculated results are shown in Fig. 11, where it can be seen that the peak ratio varies least markedly for Ar_2^+ : an effect due mainly to instrumental discrimination (core sampling). As the cluster ions increase in size, the sensitivity towards variations in β becomes more pronounced, which in turn yields more accurate values. By comparing the ratio of wings obtained from the two experimental polarizations with the simulated ratios it was possible to determine approximate values for β for the Ar_n^+ , Kr_n^+ , and Xe_n^+ data sets. These results are given in Table II and can be seen graphically in Fig. 12. For argon, the average value for β was found to be approximately +1.3, however, the actual range varies between +0.4 and +1.6. Similar variations are found for both krypton and xenon with fluctuations which suggest a different character for each cluster series studied. The β values of argon and krypton are seen to follow each other quite closely for $n \leq 10$. The oscillations seen in both rare gases at $n=3, 6$, and 9 would suggest systematic changes in structure which influence either the nature of the transition dipole or the relationship between μ and the ejected atom. It is interesting to note that these oscillations coincide with small shifts observed by both Levinger *et al.*¹ and Harberland *et al.*¹⁹ in the optical excitation spectra of small argon clusters.

Of the values for β determined for the larger clusters, those given for Ar_{15}^+ and Ar_{20}^+ are probably the most interesting and warrant further discussion. The first evidence of a significant size-dependent change in argon clusters ions at around Ar_{15}^+ came as a result of the measurements on photodissociation spectra by Levinger *et al.*¹ The presence of a substantial redshift in the absorption maximum at $n \approx 15$ was later confirmed by Harberland *et al.*¹⁹ Calculations by Ikegami and Iwata²⁴ have subsequently attributed the shift to an increase in the interaction energy between the ion core and the surrounding solvent atoms. Since β is sensitive to changes in both electronic configuration and structure, it is

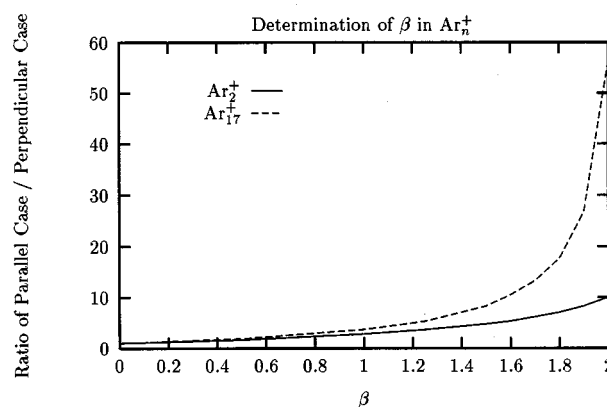


FIG. 11. Simulated ratio of fast neutrals seen at two angles of polarization of the laser radiation (parallel/perpendicular), and calculated as a function of the anisotropy parameter (β). Data for Ar_2^+ are shown thus: —, and data for Ar_{17}^+ are shown thus: - - -. The ratio starts at 1.0 for $\beta=0$.

clear that the changes identified by Ikegami and Iwata²⁴ should be expected to reveal themselves in the atom scattering patterns. In the case of Ar_{20}^+ , the dramatic drop in the value of β can probably be attributed to a change in structure. Calculations and experiment^{19,25,26} suggest that the most stable form of the cluster consists of a nineteen atom icosahedral core with the additional atom located in the second solvation shell. Under those circumstances there might be some loss of correlation between orientation of the transition dipole, μ , and the direction taken by the fast atom. Particularly, if the latter acquires kinetic energy by momentum transfer from an excited inner shell of atoms. By analogy, the relatively high values of β determined for Ar_{18}^+ and Ar_{19}^+ , could be attributed to the ejection of very specific atoms from a rigid argon lattice. The changes in experimental

TABLE II. Summary of the values determined for the anisotropy parameter (β) using the experimental data in conjunction with the simulation procedure outlined in the text. The estimated error is less than 5%.

Cluster (n)	Anisotropy parameter β					
	Photon energy 2.33 eV			Photon energy 3.5 eV		
	Ar_n^+	Kr_n^+	Xe_n^+	Ar_n^+	Kr_n^+	Xe_n^+
3	0.90	1.09	1.26	0.97	0.48	1.02
4	1.20	1.32	1.11	0.55	0.14	...
5	1.19	1.12	1.02	1.25
6	0.85	0.99	1.21
7	1.33	1.15	1.10
8	1.35	0.93	1.05
9	0.95	0.42	1.13
10	1.11	0.67	1.13
11	1.33	0.20	0.77
12	1.48	0.72
13	1.35	0.68
14	1.31	0.57
15	0.53
16	1.40
17	1.23
18	1.61
19	1.59
20	0.40
21	0.61

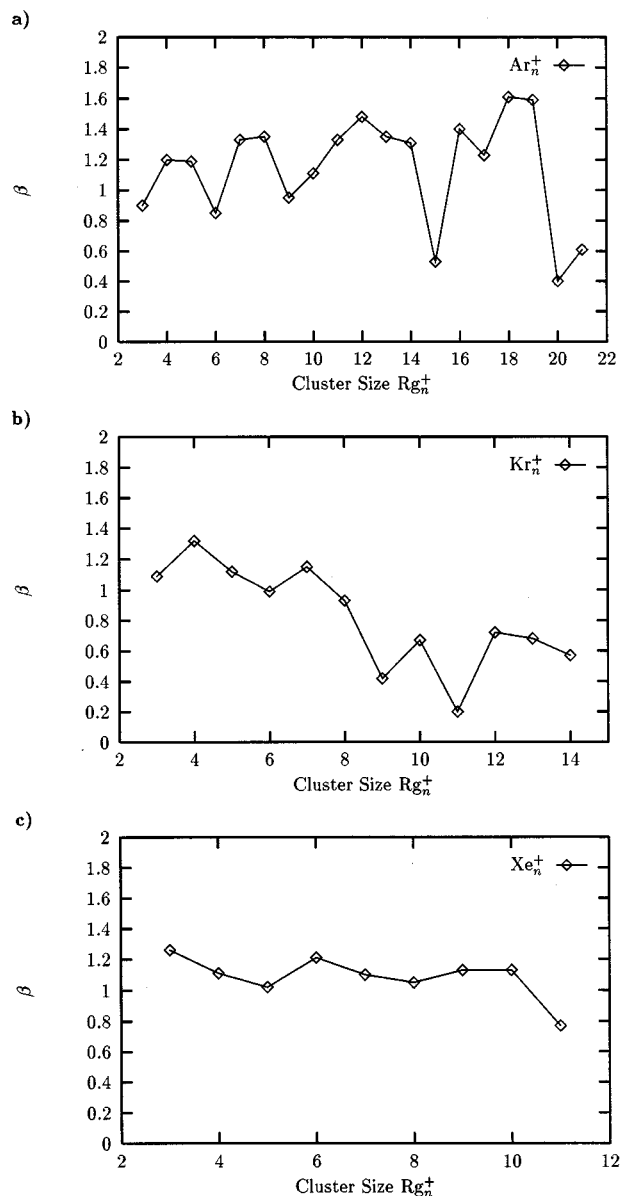


FIG. 12. Values of β plotted as a function of cluster size for the systems (a) Ar_n^+ , (b) Kr_n^+ , and (c) Xe_n^+ . In all cases the individual values were determined using the procedure outlined in the text.

behavior recorded for Ar_{15}^+ and Ar_{20}^+ , also coincide with the results of a recent series of calculations by Dottsini, Knowles, and Naumkin²⁷ where the charge distributions in these two ions were found to differ from those adopted by their immediate neighbors.

Of the β values determined at the higher photon energy of 3.5 eV, those recorded for krypton appears to exhibit the most significant differences from those seen at 2.33 eV. Such behavior could be coincident with the appearance of the photofragment, Kr^+ , in the upper spin-orbit state and would, therefore, be influenced by a change in the nature of the electronic transition being promoted by photoexcitation.

VI. CONCLUSION

The primary photofragmentation event has been modelled for the systems Ar_n^+ , Kr_n^+ , and Xe_n^+ over a broad range of

cluster ion sizes. The results show the presence of a systematic pattern of behavior, whereby each cluster responds to photoexcitation by ejecting a single atom with a high kinetic energy. Measurements of the anisotropy parameter, β , as a function of cluster size and composition, show the presence of fluctuations in Ar_n^+ which can be correlated with calculated changes in cluster structure and/or electronic configuration.

ACKNOWLEDGMENTS

A. B. J. and P. R. J. would like to thank EPSRC for studentships. The development of this experiment was aided by financial support from the Paul Instrument Fund of the Royal Society. Acknowledgements are also made to Bridgette Duncombe for her contribution to the development of the simulation program and to Brian Knight in recognition of his technical support during the construction of the experiment.

- ¹N. E. Levinger, D. Ray, M. L. Alexander, and W. C. Lineberger, *J. Chem. Phys.* **89**, 5654 (1988).
- ²J. T. Snodgrass, C. M. Roehl, and M. T. Bowers, *Chem. Phys. Lett.* **159**, 10 (1989).
- ³C. A. Woodward, J. E. Upham, A. J. Stace, and J. N. Murrell, *J. Chem. Phys.* **91**, 7612 (1989).
- ⁴Z. Y. Chen, C. R. Albertoni, M. Hasegawa, R. Kuhn, and A. W. Castleman, Jr., *J. Chem. Phys.* **91**, 4019 (1989).
- ⁵T. Nagata, J. Hirokawa, T. Ikegami, T. Kondow, and S. Iwata, *Chem. Phys. Lett.* **171**, 433 (1990).
- ⁶T. Nagata, J. Hirokawa, and T. Kondow, *Chem. Phys. Lett.* **176**, 526 (1990).
- ⁷J. A. Smith, N. G. Gotts, J. F. Winkel, C. A. Woodward, A. J. Stace, and B. J. Whitaker, *J. Chem. Phys.* **97**, 397 (1992).
- ⁸N. G. Gotts, R. Hallett, J. A. Smith, and A. J. Stace, *Chem. Phys. Lett.* **181**, 491 (1991).
- ⁹T. Nagata and T. Kondow, *J. Chem. Phys.* **98**, 290 (1993).
- ¹⁰J. A. Smith, J. F. Winkel, A. B. Jones, B. J. Whitaker, and A. J. Stace, *J. Chem. Phys.* **100**, 6412 (1994).
- ¹¹H. Haberland, A. Hofmann, and B. von Issendorff, *J. Chem. Phys.* **103**, 3450 (1995).
- ¹²A. J. Stace, *J. Chem. Phys.* **93**, 6502 (1990).
- ¹³P. G. Lethbridge and A. J. Stace, *J. Chem. Phys.* **89**, 4062 (1988).
- ¹⁴R. N. Zare, *Mol. Photochem.* **4**, 1 (1972).
- ¹⁵S. Yang and R. Bersohn, *J. Chem. Phys.* **61**, 4400 (1974).
- ¹⁶C. Jonah, *J. Chem. Phys.* **55**, 1915 (1971).
- ¹⁷P. R. Jukes, A. L. Buxey, A. B. Jones, and A. J. Stace, *J. Chem. Phys.* **106**, 1367 (1997).
- ¹⁸A. B. Jones, D. Phil. thesis, University of Sussex, 1995.
- ¹⁹H. Haberland, B. von Issendorff, T. Kolar, H. Kornmeier, C. Ludewig, and A. Risch, *Phys. Rev. Lett.* **67**, 3290 (1991).
- ²⁰R. Abouaf, B. A. Huber, P. C. Cosby, R. P. Saxon, and J. T. Mosely, *J. Chem. Phys.* **68**, 2406 (1978).
- ²¹Z. Y. Chen, C. D. Cogley, J. H. Hendricks, B. D. May, and A. W. Castleman, Jr., *J. Chem. Phys.* **93**, 3215 (1990).
- ²²P. Jukes, A. Buxey, and A. J. Stace, *J. Chem. Phys.* **109**, 5803 (1998).
- ²³K. A. Trentelman, S. H. Kable, D. B. Moss, and P. L. Houston, *J. Chem. Phys.* **91**, 7498 (1989).
- ²⁴T. Ikegami and S. Iwata, *J. Chem. Phys.* **105**, 10734 (1996).
- ²⁵T. Ikegami, T. Kondow, and S. Iwata, *J. Chem. Phys.* **98**, 3038 (1993).
- ²⁶A. J. Stace and C. Moore, *Chem. Phys. Lett.* **96**, 80 (1983).
- ²⁷N. L. Dottsini, P. J. Knowles, and F. Y. Naumkin, *Mol. Phys.* **96**, 749 (1999).